Semi-Dirac and Weyl fermions in transition metal oxides

Narayan Mohanta,[1] Jong Mok Ok,[1] Jie Zhang,[1] Hu Miao,[1] Elbio Dagotto,[1,2] Ho Nyung Lee,[1] and Satoshi Okamoto[1]
[1]*Materials Science and Technology Division, Oak Ridge National Laboratory, Oak Ridge, Tennessee 37831, USA*
[2]*Department of Physics and Astronomy, The University of Tennessee, Knoxville, Tennessee 37996, USA*

(Received 14 June 2021; revised 23 October 2021; accepted 23 November 2021; published 10 December 2021)

We show that a class of compounds with $I4/mcm$ crystalline symmetry hosts three-dimensional semi-Dirac fermions. Unlike the known two-dimensional semi-Dirac points, the degeneracy of these three-dimensional semi-Dirac points is not lifted by spin-orbit coupling due to the protection by a nonsymmorphic symmetry—mirror reflection in the a-b plane and a translation along the c axis. This crystalline symmetry is found in tetragonal perovskite oxides, realizable in thin films by epitaxial strain that results in $a^0a^0c^-$-type octahedral rotation. Interestingly, with broken time-reversal symmetry, two pairs of Weyl points emerge from the semi-Dirac points within the Brillouin zone, and an additional lattice distortion leads to an enhanced intrinsic anomalous Hall effect. The ability to tune the Berry phase by epitaxial strain can be useful in novel oxide-based electronic devices.

DOI: 10.1103/PhysRevB.104.235121

I. INTRODUCTION

Protected band degeneracy continues being a fundamental topic of interest to understand the physics of various topological semimetals, e.g., Dirac, Weyl, and nodal loop semimetals [1–6]. The guiding principle to classify these topological semimetals has been the presence of one or more symmetries that allow degenerate eigenstates [7,8]. Spin-orbit coupling (SOC) lifts the degenerate eigenstates everywhere except at momenta where symmetry enforces that the matrix elements of the SOC operator vanish [9]. Since SOC is present in all materials, the implication is that unless there is a special symmetry that protects the band degeneracy, the topological nodal semimetals exist in the theoretically idealized case when SOC is zero.

Semi-Dirac fermions in two-dimensional solids connect the physics of monolayer graphene that exhibits linear band dispersion near the Dirac points and bilayer graphene that has quadratic band dispersion near the band-touching points [10,11]. The semi-Dirac points, in which both linear and quadratic band dispersions occur along different momentum directions, exist in the absence of SOC, in various systems including hexagonal lattices under a magnetic field [12], VO_2-TiO_2 heterostructures [13,14], BEDT-TTF_2I_3 salt under pressure [15], silicene oxide [16], photonic crystals [17], and Hofstadter spectrum [18]. The quadratic dispersion along one of the momentum directions leads to an enhanced density of states at low energies as compared to linear Dirac dispersion, making instabilities relatively easier to occur due to the enlarged phase space for quantum fluctuations [19]. A semi-Dirac semimetal becomes a Chern insulator, revealing quantized anomalous Hall conductivity with broken time-reversal symmetry (TRS), in the presence of SOC that opens an energy gap at the semi-Dirac point [20]. A similar Chern insulating state is also induced in a semi-Dirac semimetal with two gapless Dirac nodes by impinging a circularly polarized light [21]. In multilayer $(TiO_2)_m/(VO_2)_n$ heterostructures, the semi-Dirac point is not destroyed by SOC in a special situation when the spins are aligned along the rutile c axis [22].

However, the questions that remain open are whether there exists a natural material in which the semi-Dirac point is gapless generically when SOC is present and whether these semi-Dirac points exist in a higher dimension. Here, we show that a class of materials hosts three-dimensional (3D) gapless semi-Dirac fermions in the presence of SOC. Tetragonal perovskite oxides with $I4/mcm$ crystalline symmetry (space group 140) exhibit such 3D semi-Dirac points at a high-symmetry point, and its nonsymmorphic symmetry protects the semi-Dirac points against the gap opening by SOC. A nonsymmorphic symmetry protected two-dimensional Dirac semimetallic phase was proposed in a theoretical model [23], and subsequent studies using *ab initio* calculations in layered compounds [24,25]. Cubic perovskite oxide thin films can be transformed into the tetragonal phase to realize the $I4/mcm$ space group under epitaxial strain that produces $a^0a^0c^-$-type (in the Glazer notation) octahedral rotation [26,27]. The out-of-phase octahedral rotation brings in the nonsymmorphic symmetry: mirror reflection about the $x = 0/y = 0$ plane, translation along [001] $z \to z + 1/2$, as shown in Fig. 1(a) (for a symmetry analysis, see the Supplemental Material [28] and Ref. [29]). A consequence of the fractional translational symmetry is that the unit cell of the original symmorphic crystal is doubled. In this case, the folded back bands stick together necessarily at the Brillouin-zone boundary if the nonsymmorphic symmetry is present, even with SOC. As a particular physical realization of the $I4/mcm$ space group, we primarily focus on tetragonal $SrNbO_3$ that manifestly displays the defining characteristics of this nonsymmorphic symmetry, and a 3D semi-Dirac point appears close to the Fermi energy at a high-symmetry point P at the Brillouin-zone boundary. Three different kinds of dispersion emerge from this semi-Dirac point—linear along the P-X direction, quadratic along

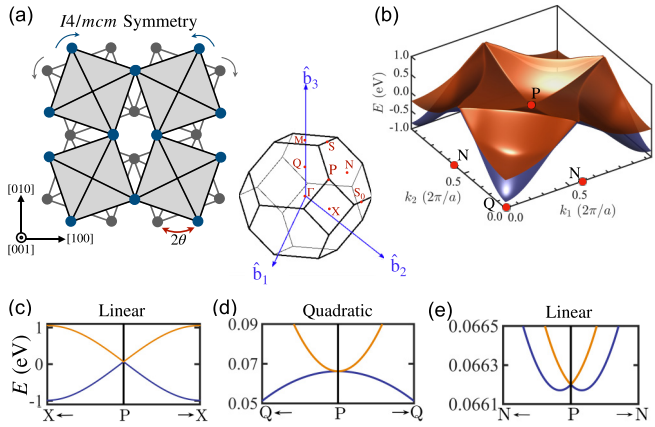

FIG. 1. (a) Illustration of the octahedral rotation-driven tetragonal phase of perovskite oxides. $a^0a^0c^-$-type rotation in a cubic crystal produces the $I4/mcm$ space group that exhibits the nonsymmorphic symmetry (mirror reflection in the a-b plane and translation along the c axis). (b) Dispersion of two electronic bands in the P-Q-N plane. (c)–(e) show the dispersion curves along different momentum paths. The inset in the middle shows the high-symmetry points in the Brillouin zone.

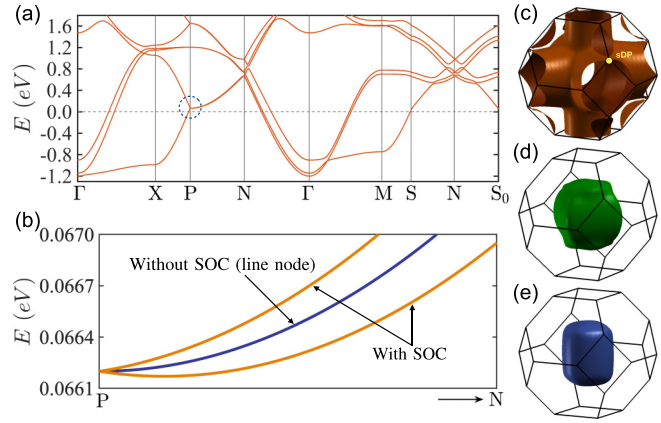

FIG. 2. (a) Band dispersion of tetragonal $SrNbO_3$ in the presence of spin-orbit coupling, through various high-symmetry momenta in the Brillouin zone. (b) Expanded view of the dispersion along the P-N direction, without and with spin-orbit coupling. (c)–(e) The three Fermi surfaces of the spin-orbit coupled t_{2g} bands at the Fermi level. The semi-Dirac point (sDP) is denoted by the dashed circle at the P point in (a) and by the yellow dot in (c).

the P-Q direction, and linear in the close vicinity of the P point along the P-N direction, as shown in Figs. 1(b)–1(e). With a TRS-breaking element such as an external magnetic field, two pairs of Weyl points appear within the Brillouin zone; each pair is shared by the opposite zone boundaries. The Weyl points in semi-Dirac semimetals lead to unique properties such as a highly anisotropic plasmon frequency, unusual carrier density dependence of the Hall coefficient, and the divergence of the ratio of orbital to spin susceptibilities at low carrier doping [30]. The Weyl points in tetragonal $SrNbO_3$ open up an energy gap with an additional broken inversion symmetry, obtained by a small displacement at a Nb site. These gapped Weyl points, at the P point, exhibit an enhanced intrinsic anomalous Hall effect. With these intriguing properties, perovskite oxides of the $I4/mcm$ space group provide a unique example of a class of compounds that hosts crystalline symmetry protected 3D semi-Dirac fermions. Our Berry curvature analysis sheds light on the unusual features in transport experiments, such as the Shubnikov–de Haas oscillations and anomalous Hall effect measurements. Furthermore, the ability to control the Berry phase by octahedral rotation shows a pathway towards developing novel electronic devices, including high-frequency rectifiers [31,32].

II. ELECTRONIC STRUCTURE

The *ab initio* band dispersion of tetragonal $SrNbO_3$ with a finite SOC along high-symmetry momenta is shown in Fig. 2(a) [28]. The t_{2g} orbitals of the Nb $4d$ state predominantly populate the Fermi level, as in the case of cubic $SrNbO_3$ [33,34]. Due to the zone folding, the bands along the P-N momentum direction are fourfold degenerate without SOC, creating line nodes. The degeneracy of these nodal lines is lifted everywhere, except at the high-symmetry points, when SOC is turned on, as shown in Fig. 2(b). The TRS and the nonsymmorphic symmetry protect the semi-Dirac degeneracy at the P point at $E \approx 0.0662$ eV. Three other Dirac points appear at the N point above $E = 0.5$ eV. Being away from the Fermi level, the Dirac points at the N point may not be accessible to transport; here, we therefore focus on the semi-Dirac point at the P point. Yet, replacing Nb with another transition metal element such as Mo can tune the Fermi level close to the Dirac points at the N point. The Fermi surfaces of the spin-orbit coupled t_{2g} orbitals are depicted in Figs. 2(c)–2(e). Due to the linear dispersion near the semi-Dirac point, a small chemical doping or gating can tune the Fermi level to the semi-Dirac point, creating the possibility to obtain a quantized Berry phase and a very high-mobility conduction [35–37]. Also, the presence of the semi-Dirac points in the asymmetric, convex Fermi surface can produce a large nonsaturating magnetoresistance [38–40].

III. TOPOLOGICAL INVARIANT

The topological properties of tetragonal $SrNbO_3$ are investigated by two protocols—first, by looking at the Berry curvature, and second, by computing the topological invariant of the Bloch bands. The Berry curvature is given by [41]

$$\Omega(\mathbf{k}) = -\sum_{m,n}^{\varepsilon_{m\mathbf{k}} \neq \varepsilon_{n\mathbf{k}}} 2\,\mathrm{Im}\frac{\langle\psi_{n\mathbf{k}}|v_x|\psi_{m\mathbf{k}}\rangle\langle\psi_{m\mathbf{k}}|v_y|\psi_{n\mathbf{k}}\rangle}{(\varepsilon_{m\mathbf{k}} - \varepsilon_{n\mathbf{k}})^2}, \qquad (1)$$

where $|\psi_{n\mathbf{k}}\rangle$ is the spinor Bloch wave function of the nth band with eigenenergy $\varepsilon_{n\mathbf{k}}$, and $\mathbf{v} = (v_x, v_y)$ is the velocity operator. We use Wannier interpolation based on maximally localized Wannier functions [42,43]. The Berry curvature in the P-N-Q plane is shown in Fig. 3(a). The semi-Dirac point, being gapless, reveals zero Berry curvature at the center P point. We introduce TRS breaking and opening of an energy gap at the semi-Dirac point by constraining to a spin polarization at the Nb sites. Figure 3(b) shows large Berry curvature contributions at and near the P point with $M = 0.2$, which represents 20% spin polarization along the $+z$ direction. M is defined as

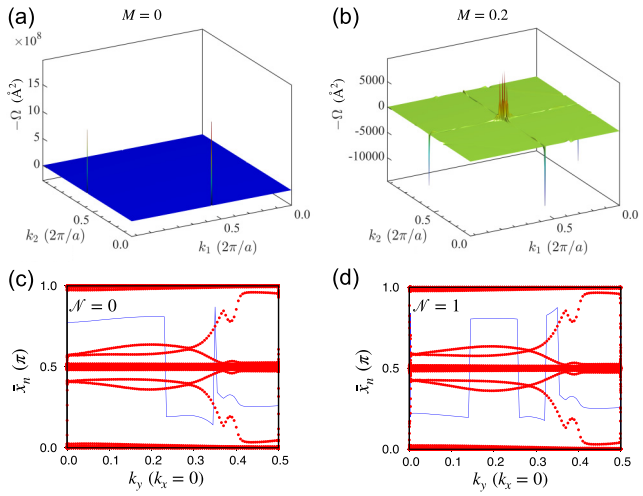

FIG. 3. Berry curvature $\Omega(\mathbf{k})$ for Nb spin polarization (a) $M = 0$, and (b) $M = 0.2$, plotted in a momentum plane containing the P point at the center, and the N points at the side centers. We use a dense 100×100 momentum grid. (c), (d) The Wannier charge centers $\bar{x}_n$ along momentum k_y with $k_x = 0$ for (a) $M = 0$, and (b) $M = 0.2$. The blue line represents the center of the maximum gap between the Wannier charge centers. In (d), the gap center crosses the Wannier charge centers an odd number of times, resulting in a topological invariant $\mathcal{N} = 1$.

$M = \sum_{a \in \text{Nb } t_{2g} \text{ orbitals}} \langle n_{a,\uparrow} \rangle - \langle n_{a,\downarrow} \rangle$, where $n_{a,\uparrow}$ is the carrier density in orbital a and spin $\uparrow$; the magnetization is compatible with the magnetic space group $4/mm'm'$. The enhanced Berry curvature induced by a nonzero M strongly suggests the nontrivial band topology. To check this possibility, we compute the topological invariant via the Wannier charge centers (WCCs) $\bar{x}_n$, corresponding to the Wannier functions that are maximally localized in one dimension, defined as [44]

$$\bar{x}_n = \frac{i}{2\pi} \int_{-\pi}^{\pi} d\mathbf{k} \langle u_{n\mathbf{k}} | \partial_{\mathbf{k}} | u_{n\mathbf{k}} \rangle, \tag{2}$$

where $|u_{n\mathbf{k}}\rangle = e^{-i\mathbf{k}\cdot\mathbf{r}} |\psi_{n\mathbf{k}}\rangle$ represents the periodic parts of the Block states. The topological invariant, originally defined in Ref. [45], can be computed from the flow of the WCCs and the largest gap between the WCCs [44]. In Figs. 3(c) and 3(d), we show the evolution of the WCCs with the momentum k_y for, respectively, $M = 0$, and $M = 0.2$. With $M = 0.2$, the center of the largest gap between the WCCs (blue line) crosses the WCCs odd number of times in traversing a path from $k_y = 0$ to $k_y = \pi/a$, yielding a topological invariant $\mathcal{N} = 1$. A nonzero $\mathcal{N}$ in a Chern insulator with broken TRS usually predicts a quantum anomalous Hall effect. We, however, find that the Hall conductivity is not quantized, and the semi-Dirac points can, therefore, be classified as type I [20], similar to those proposed in VO_2-TiO_2 heterostructures [14]. This is also verified by the absence of a band crossing of the surface states [28]. The absence of topological surface states also indicates the possibility of a fragile topological phase; it, however, requires a careful analysis of appropriate symmetry indicators [46,47].

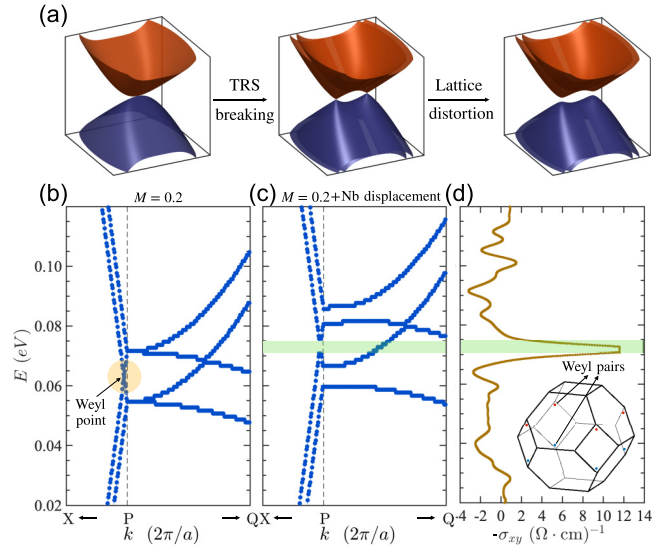

FIG. 4. (a) Effect of broken symmetries on the semi-Dirac points: TRS breaking splits the semi-Dirac point into a pair of Weyl points, and additional lattice distortion opens up an energy gap. (b) Band dispersion in the vicinity of the P point, with broken time-reversal symmetry that lifts the fourfold degeneracy of the semi-Dirac point, creating a pair of Weyl points near the P point. (c) The Weyl point acquires an energy gap with an inversion symmetry-breaking lattice distortion. (d) The anomalous Hall conductivity, with varying energy, reveals a plateau within the energy gap at the Weyl point. The inset in (d) shows the two pairs of the Weyl points in the Brillouin zone.

IV. ANOMALOUS HALL EFFECT

In the absence of TRS, e.g., with an external magnetic field, each semi-Dirac point splits into two Weyl points, as illustrated in Fig. 4(a). In the considered tetragonal $SrNbO_3$, we find that a finite magnetization at the Nb sites generates a Weyl point close to the P point, as shown in Fig. 4(b). The pair of Weyl points appears along the P-X-P momentum direction, totaling two pairs in the Brillouin zone, as shown in the inset of Fig. 4(d). The Weyl points appear when the magnetization is perpendicular to the a-b plane. Otherwise, the semi-Dirac points are directly gapped since there is no net chiral charge. By lowering the lattice symmetry further, an energy gap is induced at the Weyl points. We consider a lattice distortion that lowers the inversion symmetry but preserves the nonsymmorphic symmetry. This is achieved by shifting the center Nb site vertically by a small amount. Such a distortion may be realized naturally by epitaxial strain induced by lattice mismatch with the substrate at a polar interface, or by applying an electric field perpendicular to the interface. Figure 4(c) shows a distortion-induced energy gap at a Weyl point. Remarkably, within this energy gap, the intrinsic anomalous Hall conductivity acquires a plateau with an enhanced value, as shown in Fig. 4(d). We also find that the anomalous Hall conductivity is dependent on the amount of distortion in the tetragonal lattice and the octahedral rotation, suggesting a route to obtain tunable anomalous Hall effect in oxide interfaces.

V. TUNABLE BERRY PHASE

Understanding the Berry phase-driven phenomena in perovskite oxides is fundamentally important, not only to realize emergent electromagnetism in a feasible way, but also to identify the origin of non-trivial Hall signatures. In oxide compounds where magnetism coexists with a nontrivial band topology, such as $SrRuO_3$, the intrinsic anomalous Hall effect appears without any external magnetic field [48]. In the nonmagnetic tetragonal perovskites, such as the one considered here, i.e., $SrNbO_3$, doping magnetic impurities or applying an external magnetic field leads to a finite Berry phase in the Bloch bands. We find that the Berry curvature Ω can be tuned externally by changing the octahedral rotation angle θ [28]. Particularly, the Berry curvature and the resulting anomalous Hall conductivity vary nonmonotonically with increasing θ. Previous experiments have demonstrated that external strain can control octahedral rotations in oxide thin films [49,50]. Our results, therefore, show an effective way to control the Berry phase and the topological properties of perovskite transition metal oxides by epitaxial strain.

VI. EFFECTIVE LOW-ENERGY MODEL

To study the low-energy behavior of the 3D semi-Dirac dispersion, we derive an effective tight-binding model for the SOC-coupled t_{2g} electrons in tetragonal perovskite oxides [28]. From this tight-binding Hamiltonian, we obtain the following low-energy Hamiltonian,

$$\begin{aligned} H_{\text{low-}E} = & -2A\cos k_x \cos k_y \tau_0\sigma_0 \\ & + \tfrac{1}{2}B\tau_2(\sin 2k_x\sigma_1 - \sin 2k_y\sigma_2)\sin k_z \\ & - 2\{C(\cos k_x + \cos k_y) + D\cos k_z\}\tau_1\sigma_0 \\ & + 2E(\cos k_x + \cos k_y)\tau_2\sigma_3, \end{aligned} \tag{3}$$

where σ_i and τ_i are the Pauli matrices in the spin and the sublattice space, respectively; A, B, C, D, and E are parameters. The symmetry generators and their representations in the sublattice-spin space are $E = \tau^0\sigma^0$, $C_{2z} = i\tau^0\sigma^z$, $IC_{4z} = \tau^0(1 - i\sigma^z)/\sqrt{2}$, $IC_{4\bar{z}} = \tau^0(1 + i\sigma^z)/\sqrt{2}$, $C_{2\bar{y}}|z = i\tau^x\sigma^y$, $C_{2\bar{x}}|z = i\tau^x\sigma^x$, $M_{xy}|z = i\tau^x(\sigma^x + \sigma_y)/\sqrt{2}$, and $M_{x\bar{y}}|z = i\tau^x(\sigma^x - \sigma_y)/\sqrt{2}$.

The partial density of states surrounding the semi-Dirac point, exhibits a depletion at the energy at which the semi-Dirac point appears [28], rather than a minimum as in the isotropic Dirac or 2D semi-Dirac cases [51]. A depletion of the density of states near the Fermi energy usually indicates a strong effect of electronic correlation or disorder [52]. The mutual interplay of these additional effects in the semi-Dirac compound can, therefore, produce unconventional properties.

VII. DISCUSSION

We further analyzed the electronic properties of four other compounds from the $I4/mcm$ space group, viz., $CaNbO_3$, $SrRuO_3$, $SrMoO_3$, and $SrTiO_3$, and confirmed the presence of the 3D semi-Dirac fermions at the P point [28]. This establishes that the discussed symmetry protected band topology is generic to tetragonal perovskite oxides that belong to this space group, the only difference being the location in energy of the semi-Dirac points. For $CaNbO_3$ and $SrRuO_3$, the semi-Dirac point at the P point is closer to the Fermi level than in $SrNbO_3$. On the other hand, in $SrTiO_3$, having a large energy gap at the Fermi level, the semi-Dirac points are situated far away from the Fermi level. Using $SrTiO_3$ as a substrate is, therefore, beneficial for providing epitaxial strain. For $SrMoO_3$ and $SrRuO_3$, three Dirac points at the N point are also located close to the Fermi level which indicates that these two compounds can be interesting also to explore the nontrivial band topology.

In contrast to the isotropic Dirac semimetals, the semi-Dirac semimetals can be realized at a quantum critical point between a 3D Dirac semimetal and a topologically trivial insulator, at which both linear and nonlinear band dispersions appear [53,54]. Circularly polarized light usually does not gap the semi-Dirac nodes in rotationally invariant systems, unlike the isotropic Dirac nodes [55–57]. Tetragonal perovskite oxides, therefore, offer a feasible material platform to study new phenomena that cannot be found in known Dirac semimetals.

The interplay of Coulomb interaction and disorder in a two-dimensional semi-Dirac semimetal produces a variety of quantum phase transitions and non-Fermi liquid behaviors [58]. Disorder, particularly, has a profound effect as it can drive a Lifshitz transition from an insulator to a semimetal, and a topological transition to a Chern insulating state [59]. The interplay of topology, disorder, and Coulomb interaction in the nonsymmorphic symmetry protected semi-Dirac fermions, found in the tetragonal perovskite oxides, can lead to even richer physical properties due to their three-dimensional nature.

To conclude, we have shown that nonmagnetic tetragonal perovskite oxides with $I4/mcm$ symmetry, e.g., $SrNbO_3$, $CaNbO_3$, and $SrMoO_3$, host 3D semi-Dirac fermions that are protected by a nonsymmorphic symmetry. This crystalline symmetry can be realized by a substrate strain when the cubic perovskites undergo an octahedral rotation of type $a^0a^0c^-$. Due to the symmetry protection, the semi-Dirac degeneracy is maintained in the presence of SOC, making this class of compounds a unique, natural example. Breaking the TRS leads to two pairs of Weyl points from the semi-Dirac points. In the presence of an additional inversion symmetry-breaking lattice distortion, the Weyl points acquire an energy gap, and an enhanced intrinsic anomalous Hall effect is realized. The presence of the Weyl points can produce negative magnetoresistance induced by chiral anomaly [60]. The Berry phase at the semi-Dirac point is tunable by the octahedral rotation that can be controlled externally by sample thickness, or advanced interface engineering. Our findings serve as an important stepping stone towards understanding various kinds of quasiparticles that can be found in solids [61–65].

ACKNOWLEDGMENTS

This work was supported by the U.S. Department of Energy, Office of Science, Basic Energy Sciences, Materials Sciences and Engineering Division.

[1] C. Herring, Accidental degeneracy in the energy bands of crystals, Phys. Rev. **52**, 365 (1937).

[2] A. A. Burkov, M. D. Hook, and L. Balents, Topological nodal semimetals, Phys. Rev. B **84**, 235126 (2011).

[3] A. A. Burkov, Topological semimetals, Nat. Mater. **15**, 1145 (2016).

[4] T. Bzdušek, Q. Wu, A. Rüegg, M. Sigrist, and A. A. Soluyanov, Nodal-chain metals, Nature (London) **538**, 75 (2016).

[5] N. P. Armitage, E. J. Mele, and A. Vishwanath, Weyl and Dirac semimetals in three-dimensional solids, Rev. Mod. Phys. **90**, 015001 (2018).

[6] A. A. Burkov, Weyl metals, Annu. Rev. Condens. Matter Phys. **9**, 359 (2018).

[7] C.-K. Chiu, J. C. Y. Teo, A. P. Schnyder, and S. Ryu, Classification of topological quantum matter with symmetries, Rev. Mod. Phys. **88**, 035005 (2016).

[8] S.-Y. Yang, H. Yang, E. Derunova, S. S. P. Parkin, B. Yan, and M. N. Ali, Symmetry demanded topological nodal-line materials, Adv. Phys.: X **3**, 1414631 (2018).

[9] P. B. Allen and W. E. Pickett, Accidental degeneracy in k-space, geometrical phase, and the perturbation of π by spin-orbit interactions, Physica C: Supercond. Appl. **549**, 102 (2018).

[10] A. H. Castro Neto, F. Guinea, N. M. R. Peres, K. S. Novoselov, and A. K. Geim, The electronic properties of graphene, Rev. Mod. Phys. **81**, 109 (2009).

[11] E. McCann and M. Koshino, The electronic properties of bilayer graphene, Rep. Prog. Phys. **76**, 056503 (2013).

[12] P. Dietl, F. Piéchon, and G. Montambaux, New Magnetic Field Dependence of Landau Levels in a Graphenelike Structure, Phys. Rev. Lett. **100**, 236405 (2008).

[13] V. Pardo and W. E. Pickett, Half-Metallic Semi-Dirac-Point Generated by Quantum Confinement in TiO_2/VO_2 Nanostructures, Phys. Rev. Lett. **102**, 166803 (2009).

[14] S. Banerjee, R. R. P. Singh, V. Pardo, and W. E. Pickett, Tight-Binding Modeling and Low-Energy Behavior of the Semi-Dirac Point, Phys. Rev. Lett. **103**, 016402 (2009).

[15] S. Katayama, A. Kobayashi, and Y. Suzumura, Pressure-induced zero-gap semiconducting state in organic conductor α-(BEDT-TTF)$_2$I$_3$ salt, J. Phys. Soc. Jpn. **75**, 054705 (2006).

[16] C. Zhong, Y. Chen, Y. Xie, Y.-Y. Sun, and S. Zhang, Semi-Dirac semimetal in silicene oxide, Phys. Chem. Chem. Phys. **19**, 3820 (2017).

[17] Y. Wu, A semi-Dirac point and an electromagnetic topological transition in a dielectric photonic crystal, Opt. Express **22**, 1906 (2014).

[18] P. Delplace and G. Montambaux, Semi-Dirac point in the Hofstadter spectrum, Phys. Rev. B **82**, 035438 (2010).

[19] M. D. Uryszek, E. Christou, A. Jaefari, F. Krüger, and B. Uchoa, Quantum criticality of semi-Dirac fermions in $2+1$ dimensions, Phys. Rev. B **100**, 155101 (2019).

[20] H. Huang, Z. Liu, H. Zhang, W. Duan, and D. Vanderbilt, Emergence of a Chern-insulating state from a semi-Dirac dispersion, Phys. Rev. B **92**, 161115(R) (2015).

[21] K. Saha, Photoinduced Chern insulating states in semi-Dirac materials, Phys. Rev. B **94**, 081103(R) (2016).

[22] V. Pardo and W. E. Pickett, Metal-insulator transition through a semi-Dirac point in oxide nanostructures: VO_2 (001) layers confined within TiO_2, Phys. Rev. B **81**, 035111 (2010).

[23] S. M. Young and C. L. Kane, Dirac Semimetals in Two Dimensions, Phys. Rev. Lett. **115**, 126803 (2015).

[24] S. Li, Y. Liu, S.-S. Wang, Z.-M. Yu, S. Guan, X.-L. Sheng, Y. Yao, and S. A. Yang, Nonsymmorphic-symmetry-protected hourglass Dirac loop, nodal line, and Dirac point in bulk and monolayer X_3SiTe_6 (X = Ta, Nb), Phys. Rev. B **97**, 045131 (2018).

[25] D. Shao, T. Chen, Q. Gu, Z. Guo, P. Lu, J. Sun, L. Sheng, and D. Xing, Nonsymmorphic symmetry protected node-line semimetal in the trigonal YH_3, Sci. Rep. **8**, 1467 (2018).

[26] J. M. Rondinelli and N. A. Spaldin, Substrate coherency driven octahedral rotations in perovskite oxide films, Phys. Rev. B **82**, 113402 (2010).

[27] J. M. Ok, N. Mohanta, J. Zhang, S. Yoon, S. Okamoto, E. S. Choi, H. Zhou, M. Briggeman, P. Irvin, A. R. Lupini, Y.-Y. Pai, E. Skoropata, C. Sohn, H. Li, H. Miao, B. Lawrie, W. S. Choi, G. Eres, J. Levy, and H. N. Lee, Correlated oxide Dirac semimetal in the extreme quantum limit, Sci. Adv. **7**, eabf9631 (2021).

[28] See Supplemental Material at http://link.aps.org/supplemental/10.1103/PhysRevB.104.235121 for computational methods and additional information on the symmetry of the semi-Dirac points.

[29] M. M. Hirschmann, A. Leonhardt, B. Kilic, D. H. Fabini, and A. P. Schnyder, Symmetry-enforced band crossings in tetragonal materials: Dirac and Weyl degeneracies on points, lines, and planes, Phys. Rev. Materials **5**, 054202 (2021).

[30] S. Banerjee and W. E. Pickett, Phenomenology of a semi-Dirac semi-Weyl semimetal, Phys. Rev. B **86**, 075124 (2012).

[31] H. Isobe, S.-Y. Xu, and L. Fu, High-frequency rectification via chiral Bloch electrons, Sci. Adv. **6**, eaay2497 (2020).

[32] L. Zhang, Z. Chen, K. Zhang, L. Wang, H. Xu, L. Han, W. Guo, Y. Yang, C.-N. Kuo, C. S. Lue, D. Mondal, J. Fuji, I. Vobornik, B. Ghosh, A. Agarwal, H. Xing, X. Chen, A. Politano, and W. Lu, High-frequency rectifiers based on type-II Dirac fermions, Nat. Commun. **12**, 1584 (2021).

[33] C. Bigi, P. Orgiani, J. Sławińska, J. Fujii, J. T. Irvine, S. Picozzi, G. Panaccione, I. Vobornik, G. Rossi, D. Payne, and F. Borgatti, Direct insight into the band structure of $SrNbO_3$, Phys. Rev. Materials **4**, 025006 (2020).

[34] Y. Park, J. Roth, D. Oka, Y. Hirose, T. Hasegawa, A. Paul, A. Pogrebnyakov, V. Gopalan, T. Birol, and R. Engel-Herbert, $SrNbO_3$ as a transparent conductor in the visible and ultraviolet spectra, Commun. Phys. **3**, 102 (2020).

[35] K. Wang, D. Graf, H. Lei, S. W. Tozer, and C. Petrovic, Quantum transport of two-dimensional Dirac fermions in $SrMnBi_2$, Phys. Rev. B **84**, 220401(R) (2011).

[36] T. Liang, Q. Gibson, M. N. Ali, M. Liu, R. J. Cava, and N. P. Ong, Ultrahigh mobility and giant magnetoresistance in the Dirac semimetal Cd_3As_2 Nat. Mater. **14**, 280 (2015).

[37] M. J. Veit, R. Arras, B. J. Ramshaw, R. Pentcheva, and Y. Suzuki, Nonzero Berry phase in quantum oscillations from giant Rashba-type spin splitting in $LaTiO_3/SrTiO_3$ heterostructures, Nat. Commun. **9**, 1458 (2018).

[38] P. He, C.-H. Hsu, S. Shi, K. Cai, J. Wang, Q. Wang, G. Eda, H. Lin, V. M. Pereira, and H. Yang, Nonlinear magnetotransport shaped by Fermi surface topology and convexity, Nat. Commun. **10**, 1290 (2019).

[39] A. Vashist, R. K. Gopal, D. Srivastava, M. Karppinen, and Y. Singh, Fermi surface topology and large magnetoresistance in the topological semimetal candidate PrBi, Phys. Rev. B **99**, 245131 (2019).

[40] S. N. Zhang, Q. S. Wu, Y. Liu, and O. V. Yazyev, Magnetoresistance from Fermi surface topology, Phys. Rev. B **99**, 035142 (2019).

[41] X. Wang, J. R. Yates, I. Souza, and D. Vanderbilt, *Ab initio* calculation of the anomalous Hall conductivity by Wannier interpolation, Phys. Rev. B **74**, 195118 (2006).

[42] N. Marzari and D. Vanderbilt, Maximally localized generalized Wannier functions for composite energy bands, Phys. Rev. B **56**, 12847 (1997).

[43] I. Souza, N. Marzari, and D. Vanderbilt, Maximally localized Wannier functions for entangled energy bands, Phys. Rev. B **65**, 035109 (2001).

[44] A. A. Soluyanov and D. Vanderbilt, Computing topological invariants without inversion symmetry, Phys. Rev. B **83**, 235401 (2011).

[45] L. Fu and C. L. Kane, Time reversal polarization and a Z_2 adiabatic spin pump, Phys. Rev. B **74**, 195312 (2006).

[46] L. Elcoro, B. J. Wieder, Z. Song, Y. Xu, B. Bradlyn, and B. A. Bernevig, Magnetic topological quantum chemistry, Nat. Commun. **12**, 5965 (2021).

[47] B. J. Wieder and B. A. Bernevig, The axion insulator as a pump of fragile topology, arXiv:1810.02373.

[48] D. J. Groenendijk, C. Autieri, T. C. van Thiel, W. Brzezicki, J. R. Hortensius, D. Afanasiev, N. Gauquelin, P. Barone, K. H. W. van den Bos, S. van Aert, J. Verbeeck, A. Filippetti, S. Picozzi, M. Cuoco, and A. D. Caviglia, Berry phase engineering at oxide interfaces, Phys. Rev. Research **2**, 023404 (2020).

[49] A. Herklotz, A. T. Wong, T. Meyer, M. D. Biegalski, H. N. Lee, and T. Z. Ward, Controlling octahedral rotations in a perovskite via strain doping, Sci. Rep. **6**, 26491 (2016).

[50] A. K. Choquette, C. R. Smith, R. J. Sichel-Tissot, E. J. Moon, M. D. Scafetta, E. Di Gennaro, F. Miletto Granozio, E. Karapetrova, and S. J. May, Octahedral rotation patterns in strained $EuFeO_3$ and other *Pbnm* perovskite films: Implications for hybrid improper ferroelectricity, Phys. Rev. B **94**, 024105 (2016).

[51] W. Chen, X. Zhu, X. Zhou, and G. Zhou, Power law decay of local density of states oscillations near a line defect in a system with semi-Dirac points, Phys. Rev. B **103**, 125429 (2021).

[52] H.-J. Noh, T.-U. Nahm, J.-Y. Kim, W.-G. Park, S.-J. Oh, J.-P. Hong, and C.-O. Kim, Depletion of the density of states near the Fermi energy induced by disorder and electron correlation in alloys, Solid State Commun. **116**, 137 (2000).

[53] B.-J. Yang and N. Nagaosa, Classification of stable three-dimensional Dirac semimetals with nontrivial topology, Nat. Commun. **5**, 4898 (2014).

[54] S. A. Parameswaran, A. M. Turner, D. P. Arovas, and A. Vishwanath, Topological order and absence of band insulators at integer filling in non-symmorphic crystals, Nat. Phys. **9**, 299 (2013).

[55] A. Narayan, Floquet dynamics in two-dimensional semi-Dirac semimetals and three-dimensional Dirac semimetals, Phys. Rev. B **91**, 205445 (2015).

[56] Q. Chen, L. Du, and G. A. Fiete, Floquet band structure of a semi-Dirac system, Phys. Rev. B **97**, 035422 (2018).

[57] S. F. Islam and A. Saha, Driven conductance of an irradiated semi-Dirac material, Phys. Rev. B **98**, 235424 (2018).

[58] P.-L. Zhao, J.-R. Wang, A.-M. Wang, and G.-Z. Liu, Interplay of Coulomb interaction and disorder in a two-dimensional semi-Dirac fermion system, Phys. Rev. B **94**, 195114 (2016).

[59] P. V. Sriluckshmy, K. Saha, and R. Moessner, Interplay between topology and disorder in a two-dimensional semi-Dirac material, Phys. Rev. B **97**, 024204 (2018).

[60] D. T. Son and B. Z. Spivak, Chiral anomaly and classical negative magnetoresistance of Weyl metals, Phys. Rev. B **88**, 104412 (2013).

[61] B. Bradlyn, J. Cano, Z. Wang, M. G. Vergniory, C. Felser, R. J. Cava, and B. A. Bernevig, Beyond Dirac and Weyl fermions: Unconventional quasiparticles in conventional crystals, Science **353**, aaf5037 (2016).

[62] Z. Wang, A. Alexandradinata, R. J. Cava, and B. A. Bernevig, Hourglass fermions, Nature (London) **532**, 189 (2016).

[63] B. J. Wieder, B. Bradlyn, Z. Wang, J. Cano, Y. Kim, H.-S. D. Kim, A. M. Rappe, C. L. Kane, and B. A. Bernevig, Wallpaper fermions and the nonsymmorphic Dirac insulator, Science **361**, 246 (2018).

[64] F. Tang and X. Wan, Exhaustive construction of effective models in 1651 magnetic space groups, Phys. Rev. B **104**, 085137 (2021).

[65] Z.-M. Yu, Z. Zhang, G.-B. Liu, W. Wu, X.-P. Li, R.-W. Zhang, S. A. Yang, and Y. Yao, Encyclopedia of emergent particles in three-dimensional crystals, Sci. Bull. (2021), doi: 10.1016/j.scib.2021.10.023.